pp 1217–1238. © Royal Aeronautical Society 2017
doi: 10.1017/aer.2017.56

Integrated one-dimensional dynamic analysis methodology for space launch vehicles reflecting liquid components

J.B. Kim
J.S. Sim
ssjoon@snu.ac.kr
S.G. Lee, S.J. Shin, J.H. Park and Y. Kim
School of Mechanical and Aerospace Engineering
Seoul National University
Seoul
Republic of Korea

ABSTRACT

In this paper, structural modelling and dynamic analysis methods reflecting the characteristics of a liquid propellant were developed for a pogo analysis. The pogo phenomenon results from the complex interaction between the vehicle structural vibration in the longitudinal direction and the propulsion system. Thus, for an accurate vibration analysis of a liquid propellant launch vehicle, both the consumption of the liquid propellant and the change in the stiffness reflecting the nonlinear hydroelastic effect were simultaneously considered. A complete vehicle structure, including the liquid propellant tanks, was analytically modelled while focusing on pogo. In addition, a feasible liquid propellant tank modelling method was established to obtain an one-dimensional complete vehicle model. With these methods, comparative studies of the hydroelastic effect were conducted. Evaluations of the dynamic analysis of a reference vehicle were also conducted during the first burning stage. The numerical results obtained with the present orthotropic model and the dynamic analysis method were found to be in good agreement with the natural vibration characteristics according to previous analyses and experiments. Additionally, the reference vehicle showed the estimated occurrence of pogo in the first structural mode when compared with the frequencies of the propellant feeding system. In conclusion, the present structural modelling and modal analysis procedures can be effectively used to analyse dynamic characteristics of liquid propellant launch vehicles. These techniques are also capable of identifying the occurrence of pogo and providing design criteria related to pogo instability.

Keywords: Rocket engines; space; structural dynamics; launch vehicles; structural dynamics; pogo; hydroelastic; liquid propellant; spring-mass; longitudinal response; Saturn V; fluid structure interaction; liquid propulsion

Received 1 March 2016; revised 19 February 2017; accepted 19 April 2017; first published online 11 July 2017.

NOMENCLATURE

M	mass
K	stiffness
x	displacement in the longitudinal direction
ξ	modal displacement
Φ	mode shape
i, j	element number $i, j = 1, 2, 3, \ldots$
$\mathscr{I}$	generalized mass
ω_n	natural frequency
F	force
C	propellant consumption rate
h	height of liquid in tank
l	length of tank cylindrical section
t	time
R	radius of tank
ν	Poisson's ratio
E	Young's modulus
T	thickness of the liquid tank skin

1.0 INTRODUCTION

For a precise structural vibration analysis of a liquid propellant launch vehicle, it is required to consider the characteristics of an internal liquid propellant. There are three major reasons for this. First, consumption of the liquid propellant decreases the total weight of the launch vehicle; therefore, the natural frequencies of the complete vehicle will increase during the flight time. Second, each liquid tank of the vehicle has considerable nonlinearity due to the interaction between the internal liquid and tank structures in contact with it, known as hydroelastic properties. Therefore, the stiffness of the liquid tanks should be re-estimated by reflecting such a hydroelastic effect for an accurate vibration analysis. Finally, consumption of the liquid propellant also changes the hydroelastically affected tank area during the flight. This signifies that an estimation of the stiffness of the liquid tank during the flight will remain a complex problem to be solved. For these reasons, these two factors should simultaneously be considered for an accurate dynamic analysis of a liquid propellant launch vehicle. Figure 1 depicts this concept with reference to the dynamic characteristics of a liquid propellant launch vehicle.

The pogo phenomenon of liquid propellant launch vehicles, referring to a pogo-stick-like motion[1], requires the application of precise structural modelling and dynamic analysis methods which reflect the characteristics of the liquid propellant, as noted above. This phenomenon consists of a structure-fluid-thrust-coupled longitudinal dynamic instability arising from the interaction between the complete vehicle structure and its propulsion system. Pogo instability begins spontaneously, excites and then disappears in accordance with the specific vibration characteristics of the launch vehicle. Once it occurs, a large magnitude or long duration of vibration will bring about an engine shut-down and destruction of the equipment, and can cause injuries to astronauts. Most launch vehicles that use liquid propellants generally undergo such undesirable and harmful dynamic instability during the first burning stage of the liquid propellant. Thus, the pogo stability analysis and related

https://doi.org/10.1017/aer.2017.56 Published online by Cambridge University Press

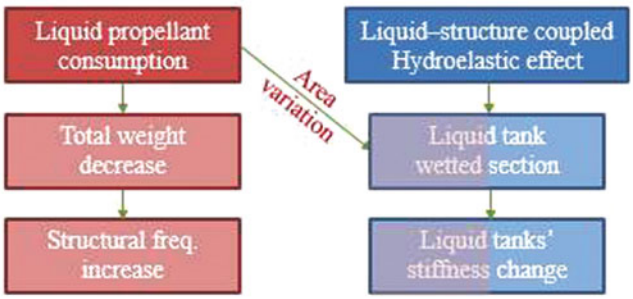

Figure 1. (Colour online) Consideration of the characteristics of a liquid propellant.

stabilizing techniques, such as the use of pogo suppression devices (PSDs), have been investigated by many researchers since the 1960s. Eventually, those efforts resorted to mathematically analysing a closed-loop feedback pogo control system. The stability analysis process for pogo requires three different analyses: a detailed structural vibration analysis, a propulsion system analysis, and a closed-loop feedback system analysis. Furthermore, each analysis involves significant nonlinearities, e.g., the liquid motion in the tank, pump cavitation, and thrust oscillation, respectively. NASA space vehicle design criteria[2-4] provided the basic mechanism and analysis/test criteria regarding this process. In addition, Rubin[5] and Oppenheim[6] presented a representative stability analysis method through a finite element analysis of a linear propulsion system.

Pogo behaviours are also related to resonance between the longitudinal structural modes at lower frequencies and the first or second modes of the propellant feedlines. Therefore, on the premise that feedline natural frequencies are already determined by appropriate experiments, an accurate prediction of the structural longitudinal vibration modes at lower frequencies will allow techniques which efficiently prevent pogo instability. With structural vibration analysis methods of the liquid propellant launch vehicle in the preliminary design phase, it will be possible to make accurate predictions of the longitudinal natural frequencies and mode shapes, ultimately to avoid dynamic instability efficiently.

Thus, this paper concentrates on structural modelling and dynamic analysis methods which take into account the liquid-structure hydroelastic effects and the degree of liquid propellant consumption. The inclusion of such effects requires special treatment that transforms the nonlinearities of the liquid motion into linear analytical equations. Analytical and experimental studies using an equivalent one-dimensional spring-mass model[7-19], a two-dimensional shell element model[20-23], and a three-dimensional finite element model[24] for liquid propellant launch vehicles and a liquid tank are sourced from earlier work.

The purpose of this paper will be to establish precise vibration analysis methods of a complete liquid propellant launch vehicle for a pogo analysis. For such a purpose, comparative studies will be conducted to analyse the hydroelastic effect on the liquid tank structure and on complete vehicles. Moreover, through comparisons with earlier liquid tank modelling methods, an adequate liquid tank modelling method will be applied to a complete vehicle analysis model. Subsequently, the natural frequencies for the lowest four modes of the reference vehicle will be obtained by considering the transient liquid consumption and the change in the stiffness of the liquid tanks due to the hydroelastic effect with dynamic analysis computational tools which are introduced here. Finally, an intuitive pogo estimation process will be carried out by comparing the presently obtained structural vibration mode

https://doi.org/10.1017/aer.2017.56 Published online by Cambridge University Press

Table 1
First-stage pogo occurrence data of earlier vehicles[28,31]

	Titan II	Gemini V	Atlas	Saturn V
Frequency	~1013 Hz	~1011 Hz	~56 Hz	~56 Hz
Maximum Amplitude	±2.5 g	±0.38 g	±0.5 g	±0.6 g
Time Duration	After ~90 sec	~92–138 sec	After ~20 sec	~105–140 sec

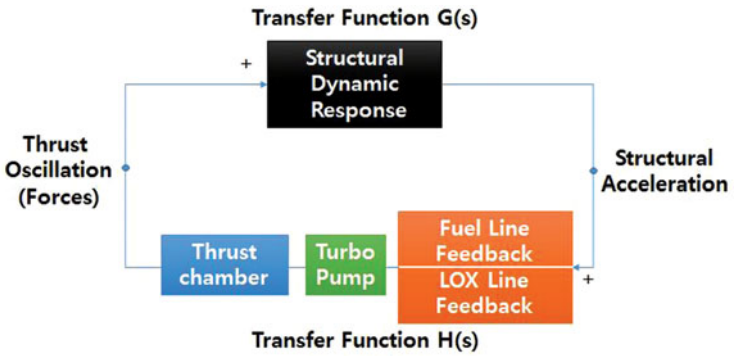

Figure 2. (Colour online) Closed-loop feedback system for the pogo instability mechanism.

and the previously acquired pogo frequency results of flight tests. Consequently, an accurate prediction of the longitudinal structural vibration characteristics will ultimately prevent pogo instability efficiently in the preliminary design phase.

2.0 METHODOLOGY OF THE STRUCTURAL MODELLING AND DYNAMIC ANALYSIS OF POGO

2.1 Mechanism of pogo and control methods

To investigate the structural modelling and analysis methods, it is necessary to understand the mechanism of the pogo phenomenon and its control methods through a closed-loop feedback system first.

The first-stage pogo occurrence results of several launch vehicles in terms of the frequencies and time durations are summarized in Table 1. It is revealed that the pogo phenomenon occurred for each vehicle in slightly different conditions which were specifically related to the characteristics of the structure and the propulsion system of the vehicle in question. However, all of these incidents were brought about by an identical mechanism, as shown in Fig. 2. The mechanism of pogo shown in Fig. 2 is an analytical process of the closed-loop system which consists of a structural and propulsion systems as represented by the transfer functions $H(s)$ and $G(s)$. When compared to the figure suggested in Rubin[5], the feedline transfer function is divided into LOX and the fuel feedline, and a turbo pump and thrust chamber are added to represent in more detail the pogo mechanism. For the pogo stability analysis, the basic assumption applied along with the linear time-invariant system is

https://doi.org/10.1017/aer.2017.56 Published online by Cambridge University Press

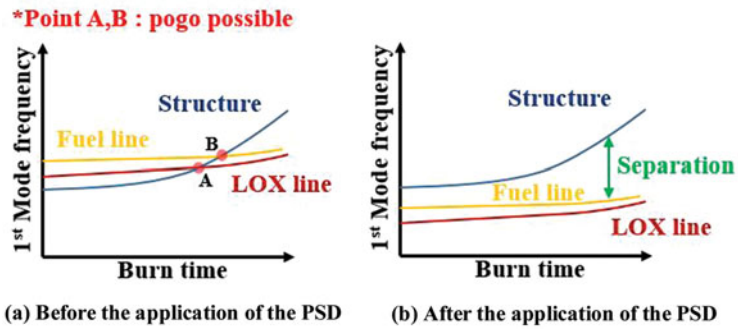

Figure 3. (Colour online) Pogo frequency control using a PSD.

that the propellant in the feedlines and engine components should be "frozen in place." In addition, the main propellant tank has a boundary condition of a zero outflow.

Given that a decrease of the propellant mass causes the natural frequencies of the structural modes for the complete vehicle to increase, structural modes will become superimposed on the propellant feedline modes at one instance during flight. Therefore, the structural mode becomes coupled to the feedline mode (i.e., LOx or fuel respectively) through the engine thrust feedback. Thus, the positive feedback of the closed loop represents strong pressure fluctuations in the propulsion system, such as the LOx feedline, fuel feedline, and pump cavitation. This then causes thrust oscillations, which affect the structural vibration relationship again. In conclusion, the longitudinal vibration resonance of the vehicle structure and feedline disturb the propulsion system, after which the thrust oscillation intensifies the original vibration. Moreover, the pressure and flow fluctuation in the propulsion system cause a loss of the propulsion performance.

If the stability analysis indicates the possibility of the occurrence of pogo, a preventive device will be required to ensure the structural integrity of the vehicle and the safety of the astronauts. To avoid excessive vibration, it will be necessary to determine whether or not the frequencies of the propellant feeding system are close to one of the natural frequencies of the structure. The basic criterion of pogo control is to separate the feedline resonant frequencies from those of the dominant structural frequencies. For that purpose, a minor modification on the vehicle structure, such as additional damping upon the fuselage structure, will either increase or decrease the severity of the vibration. The use of a passive control method which utilizes a pogo suppression device (PSD) as a type of accumulator is a common and cost-effective strategy. The PSD is typically located at the point between the feedlines and the pump inlet. Figure 3 shows the pogo frequency control approach using a PSD as an example. This method is designed to augment the stability of the system.

2.2 Complete vehicle modelling and dynamic analysis

The dynamic analysis of the structure requires the determination of the modal characteristics of the vehicle as the first step in the forced vibration-response analysis given that the natural vibration characteristics of the complete vehicle are integral to a proper understanding of the dynamic acceleration, velocity, and displacement in certain environments. However, launch vehicles using a liquid propellant are complicated to model and analyse due to the motion of the liquid and to fuel consumption, as noted above. Furthermore, the complex and massive configuration of the vehicle makes it difficult to analyse using a three-dimensional

https://doi.org/10.1017/aer.2017.56 Published online by Cambridge University Press

finite element model. Thus, to determine the longitudinal modal characteristics of the liquid propellant launch vehicle, adequate structural modelling methods need to be established. In the case of Saturn V[25], a few different analytical models were attempted for its vibration analysis.

The modal analysis method is used herein to solve the free-free axisymmetric equation of motion through an eigenvalue analysis. The complete vehicle equation of motion is obtained as a set of governing equations by considering the degree of force equilibrium. First, the mass matrix, (M) and the stiffness matrix (K) are obtained by going through structural modelling. After the modal analysis is completed, the system will be reformulated in terms of the mode shapes (ϕ), further expressed in the generalized coordinates with the modal displacements $\{\xi\}$. The final equation will therefore contain the generalized mass and the natural frequencies.

In this paper, a one-dimensional spring-mass modelling method is used for the structural modelling and dynamic analysis. This method was selected for the following reason. First, the liquid propellant launch vehicle consists of complex structures and subsystems. In contrast, the stages of a vehicle typically involve a cylindrical membrane shell and other elements, such as a liquid propellant, engines, payloads and other equipment. Therefore, a simple idealization method will be useful when concentrating only on a few dominant subsystems, such as an element of an equivalent spring-mass model, i.e., a major mass component, major structural element and liquid fuel. Second, most research on pogo vibration focuses on the lower longitudinal modes during the first-stage burn-out process.

Therefore, for efficient computations, a simplified analytical structural model is required rather than computations which simultaneously consider higher or lateral modes. Lastly, most structural modelling and analyses are usually conducted during the early phase of development such as in the preliminary design phase in which most of the detailed structural designs are not yet defined, making it difficult at this point to create a more detailed finite element model and to conduct parametric studies. This adequate model will provide sufficiently accurate results for the natural longitudinal modes in order to identify possible pogo occurrence areas and provide intuitive design criteria with regard to pogo instability. Figure 4 shows the typical one-dimensional spring-mass model for the liquid propellant launch vehicle for the purposes of this study.

The spring-mass modelling of a complete aerospace vehicle has three basic procedures, as follows. First, a concentrated mass only corresponds to one-half of the basic section of the vehicle mass. Second, these masses are connected by a massless spring with the constant $K = EA/l$, which represents the structural stiffness of the substructure. Last, superposition when representing the branches allows for uncoupled sub-elements such as engines, payloads and the liquid propellant.

Simplification of an analytical model for a launch vehicle requires comprehensive knowledge of the structure, because the accuracy of the analysis of the vibration characteristics of the vehicle depends considerably on the adequacy of the dynamic matrices consisting of the mass distribution matrix (M) and stiffness distribution matrix (K).

The creation of the mass distribution matrix (M) is relatively simple, as the mass of each element M_i is simply created by positioning the elements at their 'i-th' diagonal positions after modelling the mass distribution to 'i' elements. When a time-varying dynamic analysis of the flight time is required, the liquid propellant mass elements, M_{LOX} and M_{fuel}, will be replaced with $M_{LOx}(t)$ and $M_{fuel}(t)$, which correspondingly reflect the propellant consumption rate C_{LOx} and C_{fuel}. Additionally, if there are certain jettison structures during the main engine burning time, e.g., the fairing and booster engine, $M_{jettison}$ can assume a value of zero from the complete matrix (M). This process is shown in Figure 5.

https://doi.org/10.1017/aer.2017.56 Published online by Cambridge University Press

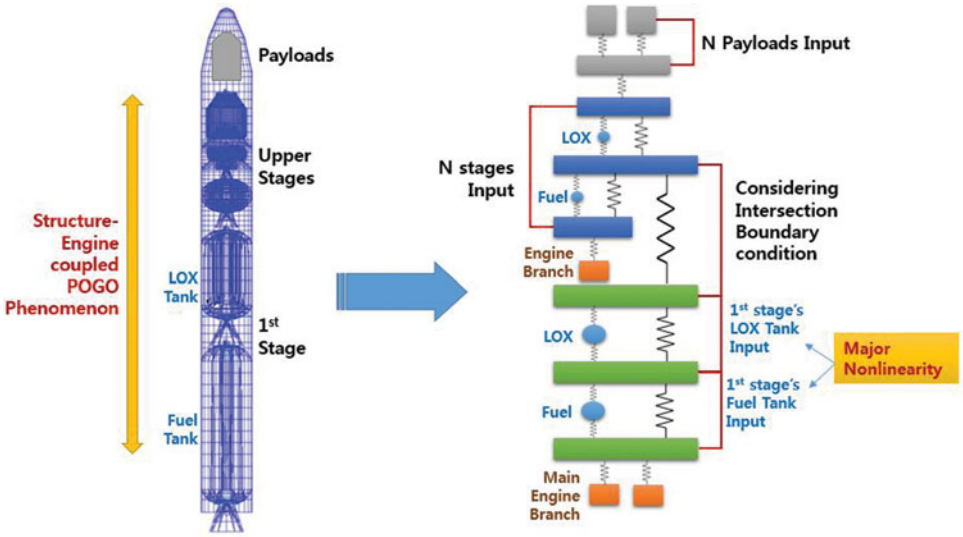

Figure 4. (Colour online) 1-D longitudinal spring-mass model of the liquid propellant launch vehicle.

Figure 5. (Colour online) Creation of the time-varying mass distribution matrix.

As compared with the mass matrix, it is more complex to create a complete stiffness distribution (K) for a dynamic analysis. Thus, the stiffness superposition and addition method, from the force equilibrium, is required to make the formation simple and straightforward[14].

Generally, each stage of the vehicle has two liquid propellant tanks, the LOx tank and the fuel tank, in a tandem array. Each tank is designed in a different shape and with a different propellant consumption rate. In addition, the mass of the liquid propellant and the tank structure is typically greater than 70% of the total vehicle mass. Thus, the stiffness of liquid propellant tanks will have a greater effect during the complete vehicle structural analysis. Moreover, derivation of the liquid tank modelling method for the dynamic analysis has been suggested in earlier works with a variety of mathematical and experimental methods[7-23]. Detailed linear modelling methods for these tanks will be presented in the next section.

The inclusion of the hydroelastic effect requires an advanced process for linearization. The hydrostatic pressure created by the effective weight of the accelerating propellant causes the tank wall to bulge in the form of a truncated cone. The shift of the centre of gravity of the liquid mass is then expressed by three springs with the constants K_1, K_2 and K_3. This set of stiffnesses should be considered with the portion of the wetted and unwetted tank sections due to the hydroelastic effect. When a time-varying dynamic analysis is also required, the liquid propellant tank stiffness values, $K_{LOx\,1,2,3}$ and $K_{fuel\,1,2,3}$, will be replaced by $K_{LOx\,1,2,3}\,(t)$ and $K_{fuel\,1,2,3}(t)$, which reflect the propellant consumption rate C and the stiffness variation regarding the amount of fluid in the tank. However, the amount of fluid and the liquid tank stiffness variation are related to the liquid height h and the total tank length l. Thus, the

https://doi.org/10.1017/aer.2017.56 Published online by Cambridge University Press

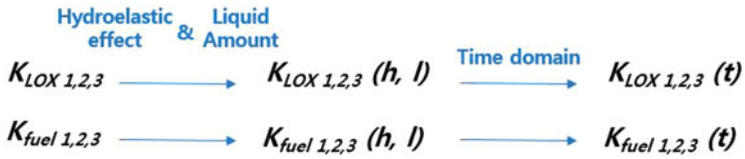

Figure 6. (Colour online) Creation of the time-varying stiffness distribution matrix.

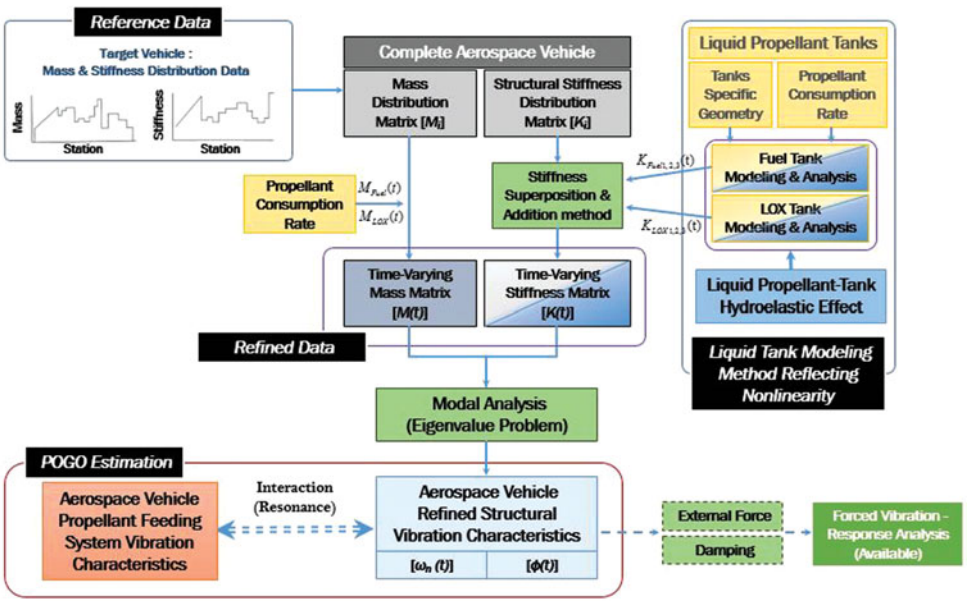

Figure 7. (Colour online) Present structural modelling and dynamic analysis reflecting a liquid propellant.

stiffness converted from the liquid domain to the time domain for the modal analysis is expressed by Equation (1). This process is also shown in Fig. 6.

$$\frac{C.t}{m_{\text{total}}} = \frac{h}{l}, \quad h = \frac{l.C}{m_{\text{total}}}.t \qquad \ldots (1)$$

In conclusion, a pogo instability analysis requires accurate time-varying natural frequencies ($w_n(t)$) and an accurate mode shape ($\phi(t)$) during the flight time. This is due to that the natural frequencies in the lower modes, which is the major factors affecting pogo instability, increase with the consumption of the liquid propellant. Therefore, with these complete vehicle structural modelling and dynamic analysis methods, the refined stiffness matrix ($K(t)$) and the refined mass matrix ($M(t)$) can be obtained. Figure 7 shows schematically this complex procedure obtained from the present computational tools for a precise vibration analysis. First, the distributions of mass and stiffness need to be provided in the longitudinal direction. The lumped masses and one-dimensional springs are allocated based on such distribution. The heavy-weight components which are less influential on the global structural dynamic characteristics, such as payload, instrument and engine, are modelled as lumped masses. The external shell and fairing are divided into two lumped masses and a one-dimensional spring.

https://doi.org/10.1017/aer.2017.56 Published online by Cambridge University Press

The tanks and propellant are idealized in the following way: the complete launch vehicle is finally converted into one mass and one stiffness matrix. In order to conduct the modal analysis, the eigenvalue analysis is required by using those two matrices.

Moreover, the proposed longitudinal one-dimensional spring-mass modelling and dynamic analysis method can also be applied to two- or three-dimensional liquid propellant tank models by replacing some of the elements with those from a one-dimensional tank model. Subsequently, pogo estimation can be conducted through a comparison with the propulsion system vibration characteristics. In addition, by applying external force and damping parameters, a forced vibration-response analysis is also possible.

3.0 COMPARISON AND APPLICATION OF THE LIQUID PROPELLANT TANK MODEL

The stiffness of the liquid propellant tanks will have a greater influence on the determination of the complete vehicle structural analysis. Moreover, derivation of a liquid tank modelling method for a dynamic analysis has been suggested in earlier work with a variety of mathematical and experimental methods[7-23]. This section discusses two approaches concerning a modelling method for a partially filled liquid propellant tank. First, various modelling methods suggested in the literature will be introduced and evaluated. Second, an adequate liquid tank modelling method for a pogo analysis will be established. The relevant method should adequately present the variation of the liquid-structure coupled stiffness to determine the free-free longitudinal vibration characteristics during the first-stage burn, as shown in Fig. 7.

Most of the previous methods begin with the basic assumption that the fluid inside the tank is rigid, incompressible and inviscid. The concept of the linearization of liquid longitudinal motion regarding the hydroelastic effect was explained in the previous section using three massless springs. A typical liquid propellant tank consists of axisymmetric and cylindrical thin-membrane shell structures. The tank structure is divided into three sections: the upper bulkhead, the cylindrical wall and the lower bulkhead. In addition, wetted and unwetted sections should be distinguished, as they have different stiffnesses depending on the remaining hydroelastic effect during the burning process.

A one-dimensional spring-mass modelling method[7-19] was developed by Wood, Pinson and Glaser. The spring-mass model mathematically uses the lumped masses and linear massless springs. Moreover, in their study they presented a means of establishing a basic spring-mass liquid tank model and reflecting an elastic bulkhead and reinforcing structures, e.g., a stringer or baffle to prevent lateral sloshing motion. Such an approach has become the basic theory of the relationship between the hydroelastic effect and tank the structures, and a rigorous analysis of this method was reported later (Refs 7 and 8). In addition, mainly in the analysis of wetted sections, the lower frequencies obtained by this spring-mass tank model are in relatively good agreement with the results of previous analyses and experiments. Figure 8 shows a basic cylindrical liquid tank model (a) and an equivalent longitudinal spring-mass model reflecting the hydroelastic effect with reinforced stringers (b).

A two-dimensional shell modelling method was developed by Archer and Rubin[20-23]. This method offers an improvement for vibration at higher modes and for the representation of the movement of the liquid. Its corresponding shell model describes a vehicle structure as a complicated set consisting of an orthotropic shell element, a fluid mass element and a spring-mass element using Rayleigh-Ritz methods. It is a more improved approach as well for the

https://doi.org/10.1017/aer.2017.56 Published online by Cambridge University Press

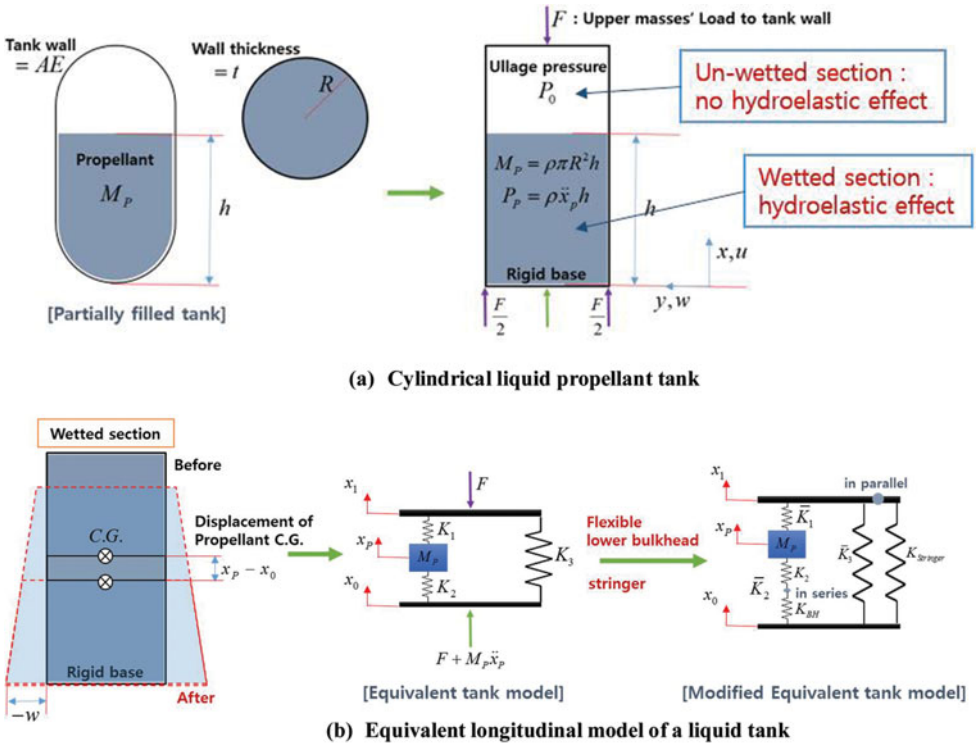

Figure 8. (Colour online) Basic one-dimensional liquid propellant tank modelling.

liquid behaviour and tank flexibility. A primary achievement of the two-dimensional model is that it presents a more rational treatment of the propellant motion than the spring-mass model[21]. Furthermore, one of the latest technologies, the three-dimensional tank modelling method, was introduced by Xu et al[24]. It deals with a deformable three-dimensional tank with the flexibility of a liquid tank taken into consideration. It provides a more accurate relationship between the oscillatory pressure and outflow near the tank outlet for a pogo stability analysis with a three-dimensional finite element model. However, such methods are rather more complex and are unsuitable when specific vehicle information is insufficient.

Although these two- and three-dimensional finite element methods exist for an analysis of a complex shell element, the problem of how correctly to represent the liquid remains. Moreover, relevant parametric studies can become time-consuming. Consequently, for studies in which detailed geometry data of the structure are insufficient, the one-dimensional spring-mass modelling method will still be effective and appropriate for a pogo analysis in the preliminary design phase. Therefore, the one-dimensional spring-mass tank modelling methods will be used in a parametric study of the hydroelastic effect and to establish an adequate tank modelling method for a pogo analysis in this paper.

The methods suggested in Wood[7] and Pinson[8] are selected and combined to investigate the hydroelastic effect of the cylindrical tank wall stiffness, lower bulkhead and stiffened stringers. Wood's method focused on the deformation of a cylinder wall, which was idealized as a truncated wall. Pinson's method focused on the wetted section and bulkhead. Membrane

https://doi.org/10.1017/aer.2017.56 Published online by Cambridge University Press

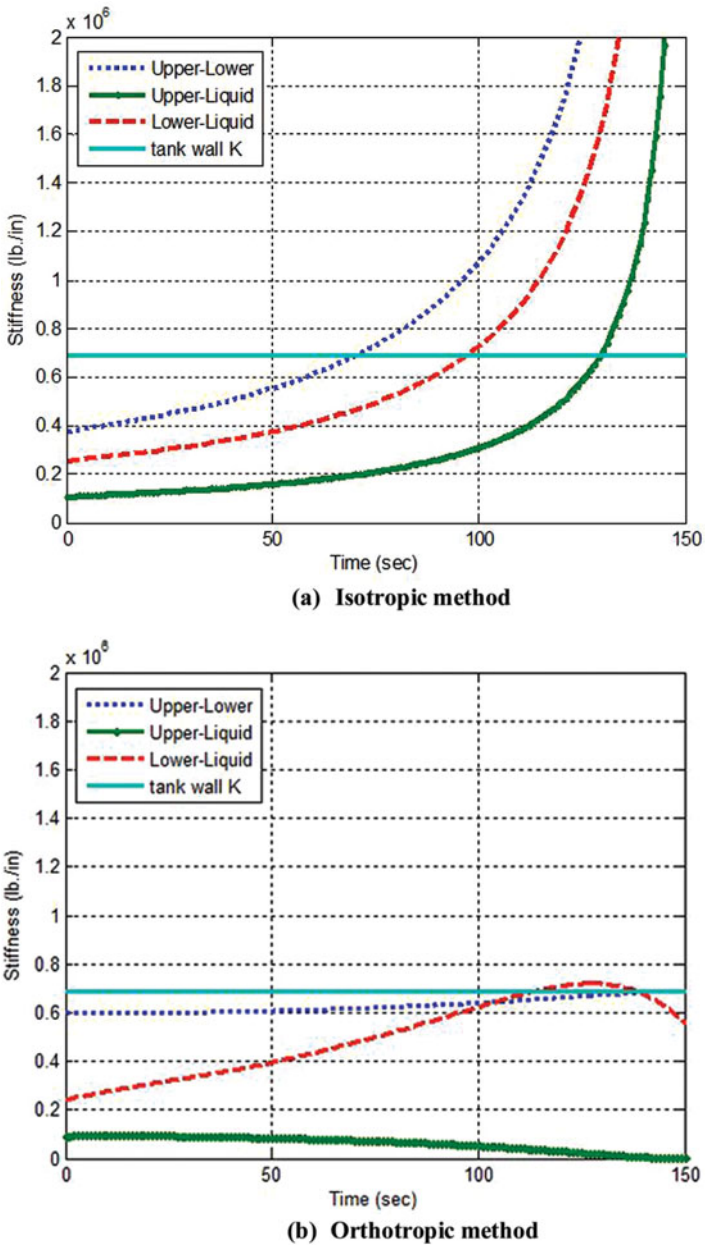

Figure 9. (Colour online) Variation of the liquid propellant tank stiffness during the burning time.

theory is used to describe the motions of the shells connected by equivalent massless springs, as shown in Fig. 8.

The stiffness of a cylindrical tank skin without the hydroelastic effect K and the stiffnesses of three liquid tanks including the hydroelastic effects, K_1, K_2 and K_3, are expressed as

https://doi.org/10.1017/aer.2017.56 Published online by Cambridge University Press

follows.

$$K = \frac{2R\pi E}{h} \quad \ldots (2)$$

$$K_1 = \left(\frac{2\upsilon}{3-2\upsilon^2}\right)K \text{ (Stiffness connecting the upper mass to the propellant mass)} \quad \ldots (3)$$

$$K_2 = \left(\frac{2-2\upsilon}{3-2\upsilon^2}\right)K \text{ (Stiffness connecting the propellant mass to the lower mass)} \quad \ldots (4)$$

$$K_3 = \left(\frac{3-2\upsilon}{3-2\upsilon^2}\right)K \text{ (Stiffness connecting the upper mass to the lower mass)} \quad \ldots (5)$$

From Equations (2)–(5), the basic linear liquid tank equation is derived simply from the radius of the tank area, the Young's modulus of the skin, the height of the liquid in tank and the Poisson's ratio of the skin.

While the stiffness of the ellipsoidal elastic lower bulkhead should be considered to increase the accuracy of the analysis, deriving new parameters and transfer functions is now required. The parameter n is the ratio of the lower bulkhead depth to the radius, $n = b/R$, and q is the ratio of the liquid height to the radius, $q = h/R$.

$H(n, \upsilon)$, $G(n, \upsilon)$, and $F(n, \upsilon)$ are the respective transfer functions of the lower bulkhead shape and Poisson's ratio. The three functions are obtained from the first moment of the volume increment, the volume increment by hydrostatic pressure, and the volume increment by constant inertial pressure, respectively. K_{BH} means the stiffness of the bulkhead.

$$K_{BH} = 2Et\pi\left(\frac{(3q+2n)^2}{9(H(n,\upsilon)+2qG(n,\upsilon)+q^2F(n,\upsilon)}\right) \quad \ldots (6)$$

Additionally, if the tank structure has a stiffened structure such as a stringer, the stiffness of any such additional structures should be considered, as follows.

$$K_{\text{stiffener}} = A_{\text{stiffener, total}}\frac{E_{\text{stiffener}}}{h_{\text{stiffener, actual}}} \quad \ldots (7)$$

Equations (2)–(7) are used in the one-dimensional tank modelling and dynamic analysis. This tank modelling method should consider the load path and spring assembly in either a parallel or series configuration. Consequently, by combining these equations, the set of liquid tank stiffnesses reflecting the hydroelastic effect is as follows.

$$K_{22} = \frac{K_2K_{BH}}{K_2+K_{BH}} \quad \text{(Stiffness connecting the propellant mass to the lower mass, in a series assembly)} \quad \ldots (8)$$

$$K_{11} = \frac{\upsilon}{1-\upsilon}K_{22} \quad \text{(Stiffness connecting the upper mass to the propellant mass, reflecting a change of } K_{22}\text{)} \quad \ldots (9)$$

https://doi.org/10.1017/aer.2017.56 Published online by Cambridge University Press

$$K_{33} = K - \upsilon K_{22} + K_{\text{stiffener}} \quad \text{(Stiffness connecting the upper mass to the lower mass, in a parallel assembly)} \qquad \ldots (10)$$

With this method, the hydroelastic effect on the tank skin and lower bulkhead can be included in the tank analytical model. However, these methods represent only the wetted section of the liquid propellant tank in a static condition. Thus, this combined methodology of Wood's and Pinson's methods is limited when used for a time-varying dynamic analysis, so in this paper, these methods are only used to conduct the parametric study of the hydroelastic effect.

Eventually, a modified one-dimensional liquid tank modelling method was investigated (see Ref. 18). The integrated structural modelling method including both wetted sections and unwetted sections was established and applied to a 1/10-scale Saturn V replica vehicle to estimate the longitudinal modes of the vehicle during the burning time of the S-IC stage.

The set of liquid tank stiffnesses is modified considerably using a 2×2 stiffness matrix (C_{ij}), which is an orthogonal matrix reflecting the elastic properties of the tank shell. It is also considered to be a more specific tank shape. Equations (11)–(14) present the methods used to calculate (C_{ij}). The parameter T is the thickness of the tank skin, A_{longi} is the average area of the longitudinal stringers in terms of the circumference, and A_{circum} denotes the average area of the circumferential stiffener in terms of the length.

$$[C_{ij}] = \begin{bmatrix} C_{11} & C_{12} \\ C_{12} & C_{22} \end{bmatrix} \qquad \ldots (11)$$

$$C_{11} = \frac{TE}{1-\upsilon^2} + A_{longi}E \qquad \ldots (12)$$

$$C_{22} = \frac{TE}{1-\upsilon^2} + A_{circum}E \qquad \ldots (13)$$

$$C_{12} = \frac{\upsilon TE}{1-\upsilon^2} \qquad \ldots (14)$$

The basic stiffness equations are now modified with new parameters, as follows. K_c refers to the modified skin stiffness of the cylindrical section.

$$K_c = \frac{2\pi R}{l} C_{11}\left(1 - \frac{{C_{12}}^2}{C_{11}C_{22}}\right) \quad \text{(cylindrical section skin stiffness)} \qquad \ldots (15)$$

$$\Gamma = 3q + 2n - \left(\frac{m^3}{n_1^2}\right) \qquad \ldots (16)$$

($n_1 = \frac{b_1}{R}$, $m = \frac{c}{R}$, b_1: upper bulkhead depth, c: liquid height in the upper bulkhead)

$$K_{BH} = 2Et\pi\left(\frac{\Gamma^2}{9(H(n,\upsilon) + 2qG(n,\upsilon) + q^2F(n,\upsilon)}\right) \qquad \ldots (17)$$

Equation (17) is an advanced expression for both the lower and upper bulkheads with Γ instead of ($3q$-$2n$), as in Equation (6). Therefore, K_1, K_2, and K_3 are derived with these

https://doi.org/10.1017/aer.2017.56 Published online by Cambridge University Press

advanced parameters, using notations identical to those used in Equations (3)–(5).

$$\Lambda = \frac{12(q^3 - m^3)}{p\Gamma^2} - 9\frac{{C_{12}}^2}{C_{11}C_{22}}\frac{(q^2 - m^2)}{p^2\Gamma^2} + \frac{2\pi}{p}\frac{C_{22}}{K_{BH}}\left(1 - \frac{{C_{12}}^2}{C_{11}C_{22}}\right) \quad \ldots(18)$$

$$K_1 = K_c\frac{C_{22}}{C_{11}}\frac{3\frac{C_{12}(q^2-m^2)}{C_{22}p\Gamma}}{\Lambda} \quad \ldots(19)$$

$$K_2 = K_c\frac{C_{22}}{C_{11}}\frac{1 - 3\frac{C_{12}(q^2-m^2)}{C_{22}p\Gamma}}{\Lambda} \quad \ldots(20)$$

$$K_3 = K_c\frac{\frac{12(q^3-m^3)}{p\Gamma^2} - 3\frac{C_{12}}{C_{11}}\frac{(q^2-m^2)}{p\Gamma} + \frac{2\pi}{p}\frac{C_{22}}{K_{BH}}\left(1 - \frac{{C_{12}}^2}{C_{11}C_{22}}\right)}{\Lambda} \quad \ldots(21)$$

($p = \frac{l}{R}$: ratio of the liquid height to the radius)

With Equations (19)–(21), the set of liquid propellant tank stiffnesses can be reflected in the unwetted section and the upper bulkhead. Thus, Equations (3)–(5) and (19)–(21) used respectively as isotropic and orthotropic computational tools for the liquid propellant tank analysis are also developed. The isotropic method reflects a rigid bulkhead of two tanks, and the orthotropic method reflects an elastic bulkhead of two tanks.

Finally, the analytical model for the time-varying dynamic analysis, as shown in Fig. 7, is established using the aforementioned advanced tank modelling method. Furthermore, the pogo instability analysis can now be conducted. This paper attempts to integrate the methodologies suggested by Wood and Pinson. The presently suggested method in this paper is integration of those two methodologies, considering both wetted and unwetted sections. Consumption of the propellant is also included. The present analysis is then conducted in time domain.

4.0 NUMERICAL RESULTS AND DISCUSSION

4.1 Comparative study of the hydroelastic effect

To analyse the interaction between the liquid and the tank structure, two comparative studies are carried out. First, the combined methodology of Wood's and Pinson's tank modelling methods is used to calculate the set of liquid tank stiffnesses under variable conditions. Second, two types of advanced time-varying tank modelling methods (i.e., isotropic and orthotropic methods, in this case) are used to analyse the hydroelastic effect on the upper and lower bulkheads during the burning time.

Initially, to analyse the hydroelastic effect on a simple tank structural model, four different case studies are conducted using the combined methodology suggested by Wood and Pinson, as listed in Table 2. Case 1 is considered with no hydroelastic effect on the liquid tank, and only the stiffness K in Equation (2) is used. Cases 2–4 consider the hydroelastic effect and the set of stiffnesses in Equations (3)–(10). Cases 2 and 3 are classified in terms of whether the lower bulkhead is rigid or elastic. Lastly, in Case 4, stiffeners are added to Case 3. The reference tank's configuration[11], as listed in Table 2, is equally applied to all of these cases.

https://doi.org/10.1017/aer.2017.56 Published online by Cambridge University Press

Table 2
Numerical result by the combination of Wood's and Pinson's methods

		Case 1: No hydroelastic effect	Case 2: Rigid bulkhead	Case 3: Elastic bulkhead	Comparison Cases 2 & 3	Case 4: adding stiffeners	Comparison Cases 3 & 4
Stiffness (lb/in)	K_1 (M_1–M_2)	5.0535×10^5	1.212×10^5	1.110×10^5	8.5% decrease	1.110×10^5	–
	K_2 (M_2–M_3)		2.426×10^5	2.220×10^5	8.5% decrease	2.220×10^5	–
	K_3 (M_1–M_3)		4.245×10^5	4.313×10^5	1.6% increase	5.171×10^5	19.9% increase
Natural frequencies (Hz)	Mode 1	0	0	0	–	0	–
	Mode 2	10.5	29.4	28.2	4.1% decrease	27.9 Hz	1.1% decrease
	Mode 3	–	71.3	71.2	0.1% decrease	75.8 Hz	6.5% increase
Target tank geometry (Atlas/ Centaur/ Surveyor first-stage LOx tank[12])	Material: aluminium and liquid oxygen Properties: $E_{skin,\ bulkhead,\ stringer} = 10^6$ psi, $\rho_{LOX} = 0.0412$ lb/ in^3 Tank specifications: thickness (BH, wall): 0.05 in liquid height: 373 in, radius: 60 in ellipsoidal bulkhead ratio (n): 0.7071 Stringer specifications: 12 aluminium stringers ($0.5 \cdot 0.5 \cdot 350$ in^3) uniform in circumferential direction weight increase 102.9 lb (0.05% increase) Mass element composition: M_1 = (upper bulkhead/half tank structure/half adapter structure) M_2 = (LOX) M_3 = (half tank structure/lower bulkhead)						

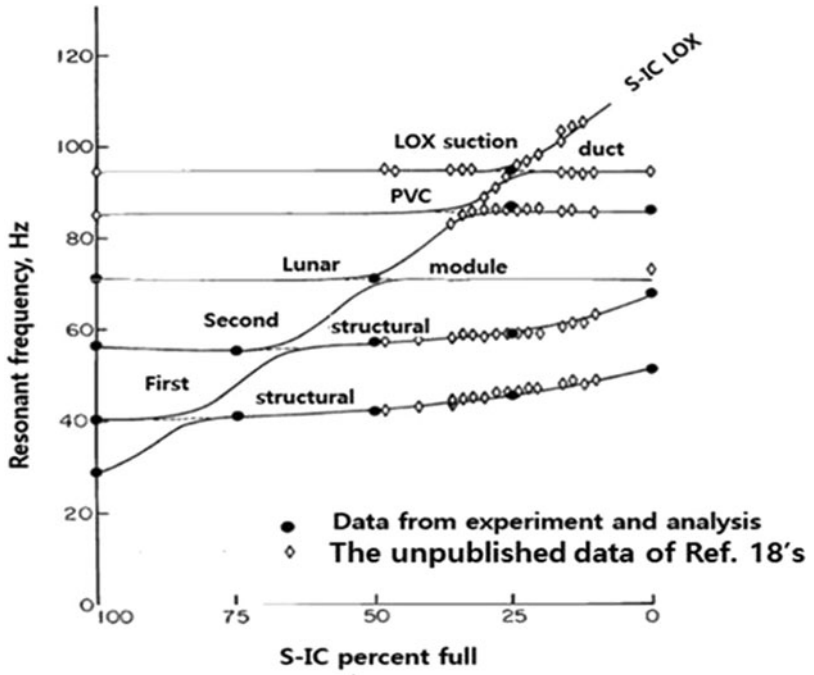

Figure 10. Estimation result of the frequencies of the 1/10-scale Saturn V replica's S-IC stage[18].

As shown in Cases 1 and 2, which are for a cylindrical wall with a rigid bulkhead, the hydroelastic effect on the liquid tank stiffness and natural frequencies are considerable. Cases 2 and 3 demonstrate that the effect of including the bulkhead elasticity brings a reduction of 8.5% of both K1 and K2 connecting the liquid element as well as an increase of 1.6% for K3. For the natural frequencies, a small decrease in Modes 2 and 3 is observed. This result suggested that the bulkhead elasticity affects the degree of tank vibration by the load path through the liquid element, not through the tank skin. In Cases 3 and 4, a stringer structure is attached to the tank skin for reinforcement in the longitudinal direction. In terms of vibration, the result of this measurement shows a considerable increase of 19.9% in K3 and an increase of 6.5% of Mode 3 with a weight increase of 0.05%. This result suggests that the stringer structure affects the tank wall stiffness considerably in spite of its small weight.

Additionally, with advanced liquid tank modelling methods, the set of liquid tank stiffnesses reflecting both the transient liquid consumption and the hydroelastic effect is obtained, as shown in Fig. 10. The reference tank is the LOx tank of the first stage of the 1/10-scale Saturn V replica[18], and time-varying analyses are conducted via isotropic and orthotropic methods, respectively. With the isotropic method (a), it is assumed that the upper and lower bulkheads are rigid, with Equations (3)–(5) used. Thus, the three values of K of the liquid tank increase continuously upon consumption of the liquid. However, in the orthotropic method (b), as a more accurate method with Equations (19)–(21), the variation of the stiffness is very different. These results suggest that the hydroelastic effect of both bulkheads is significant in the liquid propellant tank modelling.

https://doi.org/10.1017/aer.2017.56 Published online by Cambridge University Press

4.2 Dynamic analysis of a complete liquid propellant launch vehicle and pogo estimation

A comprehensive evaluation of the complete launch vehicle model and dynamic analysis method as well as the liquid propellant tank model was conducted by comparing the present computational results with the existing analytical and experimental results (Ref. 18).

Thus, the full time-varying modal analysis of the reference vehicle, the 1/10-scale Saturn V replica in Ref. 18, was conducted using the developed complete vehicle modelling method and the advanced liquid tank modelling method on different LOX and RP-1 tanks of the S-IC stage, as shown in Fig. 7. The results of the vibration analysis and from experiments on this vehicle are shown in Fig. 10. The corresponding experimental results were included in Ref. 18.

This process is conducted for three cases: the first without a hydroelastic effect, the second using an isotropic method, and the third using an orthotropic method for an accurate comparison.

As a result, the results after the application of the present methodologies are in good agreement with those of the first four modes with the natural frequencies and the analytical and experimental results in the literature (i.e., the green points), as shown in Table 3 and Fig. 11. As shown in Table 3, the difference between the literature results and the numerical results for the natural frequencies shows a decrease from 0.5–3.1% to 0.5–1.2% with the orthotropic method. In addition, the orthotropic tank modelling method is found to be more accurate—closer to the green points in Fig. 11 than the other methods. However, a difference in the numerical results is obtained with the RP-1 tank configuration data due to insufficient information. Hence, this result suggests that the orthotropic tank modelling method is nearly equivalent to actual liquid tank motion.

In addition, Fig. 10 is to illustrate the modal behaviour of a complete vehicle and the coupling between the S-IC LOx mode and the subsystem resonances. Therefore, by comparing Figs. 10 and 11(c), the obtained modal behaviour of the complete vehicle can be identified. The frequency coalescences among the two liquid tank modes, the first and second structural modes, and the subsystem resonances are significantly manifested in the S-IC stage, as shown in Fig. 10.

In conclusion, the results show that the data obtained here and the previous analytical/experimental results are well correlated, as shown in Table 3 and Figs 10 and 11.

Also, the pogo occurrence area observed from the flight test is included regarding the time and frequency, which is designated as the dark area in Fig. 12. Pogo instability was caused by the resonance between the observed frequency of the propellant system and the first longitudinal structural mode frequency. The actual pogo phenomenon was found in Saturn V AS-502 flight test data as well; the frequency is 5.0–5.6 Hz and the duration time is 110–140 sec[28]. These factors regarding the replica model and the actual vehicle must be included when devising the replica configuration prototype parametric relationship[13]. In this case, the geometric scale was 1–10 and the shell frequencies were then ten times greater. Thus, the vehicle analysed here showed the estimated pogo areas, which were located at 50–56 Hz and at 110–140 sec. Furthermore, Fig. 12 indicates an overlapped area in the first structural mode.

Consequently, it will be possible to estimate the degree of pogo stability intuitively at the preliminary design phase by applying the present complete vehicle model, the modal analysis results and the liquid propellant tank modelling method proposed in this paper.

https://doi.org/10.1017/aer.2017.56 Published online by Cambridge University Press

Table 3
Numerical result of the natural frequencies by the isotropic and orthotropic methods

Time (Propellant)	Methods	Mode 1 (Difference)	Mode 2 (Difference)	Mode 3 (Difference)	Mode 4 (Difference)	Average Difference
0 sec (100%)	Ref. 18	38.0 Hz	40.3 Hz	55.3 Hz	70.8 Hz	–
	Isotropic Method	37.9 Hz (0.3%)	39.0 Hz (3.2%)	55.1 Hz (0.4%)	70.6 Hz (0.3%)	1.0%
	Orthotropic Method	37.9 Hz (0.3%)	40.0 Hz (0.7%)	55.2 Hz (0.2%)	70.6 Hz (0.3%)	0.4%
76 sec (50%)	Ref. 18	43.1 Hz	58.2 Hz	70.8 Hz	–	–
	Isotropic Method	45.9 Hz (6.5%)	56.8 Hz (2.4%)	70.6 Hz (0.3%)	–	3.1%
	Orthotropic Method	43.5 Hz (1.0%)	56.9 Hz (2.2%)	70.6 Hz (0.3%)	–	1.2%
153 sec (0%)	Ref. 18	53.3 Hz	70.8 Hz	78.0 Hz	–	–
	Isotropic Method	53.2 Hz (0.2%)	70.6 Hz (0.3%)	77.1 Hz (1.2%)	–	0.5%
	Orthotropic Method	53.3 Hz (0%)	70.6 Hz (0.3%)	77.1 Hz (1.2%)	–	0.5%

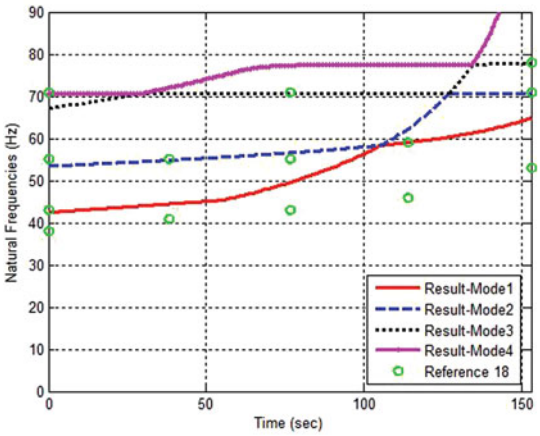

(a) No hydroelastic effect

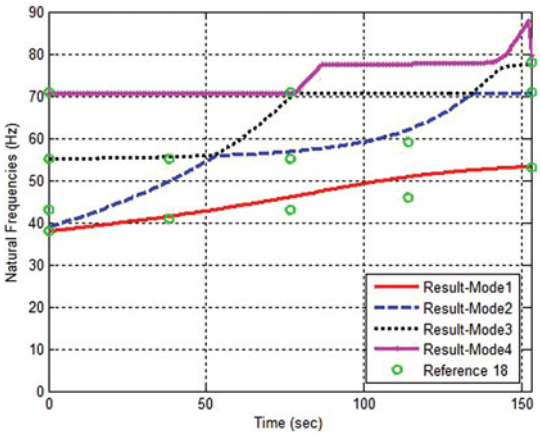

(b) Isotropic method

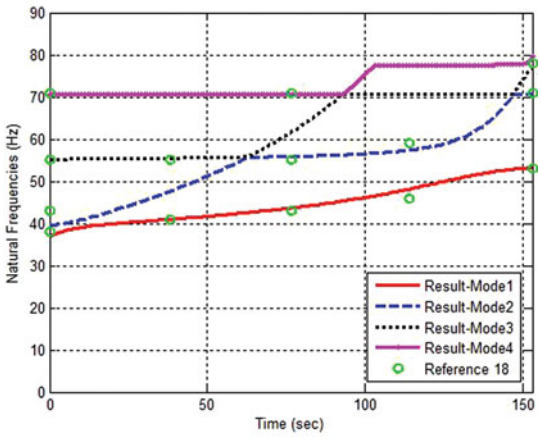

(c) Orthotropic method

Figure 11. (Colour online) Results by the present analysis for the 1/10-scale Saturn V replica model at the first stage burn.

https://doi.org/10.1017/aer.2017.56 Published online by Cambridge University Press

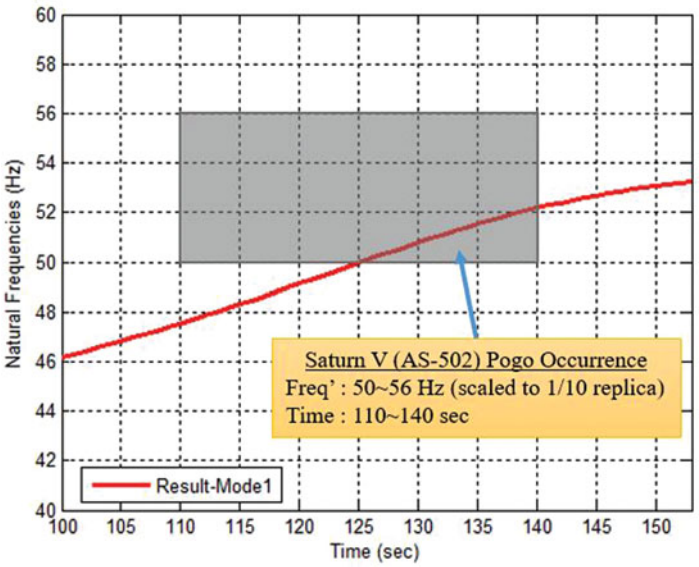

Figure 12. (Colour online) Intuitive pogo estimation result of the reference vehicle.

5.0 CONCLUSION

Most liquid propellant launch vehicles experience what is known as pogo instability. Moreover, the structure-fluid-engine coupled mechanism of the pogo phenomenon is very complex to analyse and control. Hence, precise structural modelling and dynamic analysis methods are required to analyse space launch vehicles that use a liquid propellant.

In this paper, a complete launch vehicle including liquid propellant tanks was analytically modelled for a pogo instability analysis, focusing on the longitudinal lower modes. Moreover, adequate liquid propellant tank modelling methods were established using an one-dimensional spring-mass model to devise a refined vehicle model. Subsequently, with these methods, comparative studies of the liquid propellant tank model reflecting the hydroelastic effect were conducted.

A dynamic analysis of a 1/10-scale Saturn V replica configuration was also conducted. The numerical results obtained by the orthotropic method were found to be in good agreement with the natural vibration characteristics from earlier analyses and experiments, showing a difference in the natural frequencies of ~0.5–1.2%. In addition, the reference vehicle showed pogo estimated areas in the first structural mode through a comparison of the frequency of the propellant feeding system. For effective calculations, the matrix size reduction of a complete vehicle was also investigated.

Therefore, the present structural modelling and modal analysis methods can be effectively used to analyse the vibration characteristics of launch vehicles that utilize a liquid propellant. These methods are also capable of identifying pogo occurrence areas and providing design criteria with which to assess the potential for pogo instability.

https://doi.org/10.1017/aer.2017.56 Published online by Cambridge University Press

ACKNOWLEDGEMENTS

This work was supported by the Advanced Research Centre Program (NRF-2013R1A5A1073861) through a grant from the National Research Foundation of Korea (NRF) funded by the Korean government (MSIP) as contracted through the Advanced Space Propulsion Research Centre at Seoul National University and by the program of Development of Space Core Technology through the National Research Foundation of Korea funded by the Ministry of Science, ICT and Future Planning (NRF-2015M1A3A3A05027630).

REFERENCES

1. RASUMOFF, A. and WINJE, R.A. The pogo phenomenon: Its causes and cure, *Astronautical Research*, 1971, pp 307-322.
2. Anonymous. NASA space vehicle design criteria – prevention of coupled structure-propulsion instability (POGO), NASA SP-8055, 1970.
3. Anonymous. NASA space vehicle design criteria – natural vibration modal analysis, NASA SP-8012, 1970.
4. Anonymous. NASA space vehicle design criteria – structural vibration prediction, NASA SP-8050, 1970.
5. RUBIN, S. Longitudinal instability of liquid rockets due to propulsion feedback (POGO), *J Spacecraft*, 1966, **3**, (8), pp 1188-1195.
6. OPPENHEIM, B.W. and RUBIN, S. Advanced pogo stability analysis for liquid rocket, *J Spacecraft and Rockets*, 1993, **30**, (3), pp 360-373.
7. WOOD, J.D. Survey on missile structural dynamics, EM 11-11, Vol. 1, TRW Space Technology Laboratories, 1961.
8. PINSON, L.D. Longitudinal spring constants for liquid-propellant tanks with ellipsoidal ends, NASA TN D-2220, 1964.
9. CARDEN, H.D. and RANEY, J.P. An experimental and analytical study of the longitudinal vibration of a simplified Thor vehicle structure, NASA TN-3632, 1966.
10. ABRAMSON, H.N. The dynamic behaviour of liquids in moving containers, NASA SP-106, 1966.
11. SCHETT, R.H., APPLEBY, B.A. and MARTIN, J.D. Dynamic loads analysis of space vehicle systems – launch and exit phase, GDC-DDE66-012, General Dynamics Convair Division, 1966.
12. GERUS, T.F., HOUSELY, J.A. and KUSIC, G. Atlas-Centaur-Surveyor longitudinal dynamics tests, NASA TM X-1459, 1967.
13. LEADBETTER, S.A., LEONARD, H.W. and BROCK, E.J. Design and fabrication considerations for a 1/10-scale replica model of the Apollo/Saturn V, NASA TN D-4138, 1967.
14. STALEY, J. A. Dynamic stability of space vehicles Vol. II – determination of longitudinal vibration modes, NASA CR-936, 1967.
15. WINGATE, R.T. Matrix analysis of longitudinal and torsional vibrations in nonuniform multibranch beams, NASA TN D-3844, 1967.
16. PENGELLEY, C.D. Natural frequency of longitudinal modes of liquid propellant space launch vehicles, *J Spacecraft*, 1968, **5**, (12), pp 1425-1431.
17. GLASER, R.F. Longitudinal mass-spring modelling of launch vehicles, NASA TN D-5371, 1969.
18. PINSON, L.D. and LEONARD, H.W. Longitudinal vibration characteristics of 1/10-scale Apollo/Saturn V replica model, NASA TN D-5159, 1969.
19. GLASER, R.F. Analysis of axisymmetric vibration of a partially liquid-filled elastic sphere by the method of Green's function, NASA TN D-7472, 1973.
20. ARCHER, J.S. and RUBIN, C.P. Improved analytical longitudinal response analysis for axisymmetric launch vehicles, NASA CR-345, 1965.
21. PINSON, L.D. Evaluation of a finite-element analysis for longitudinal vibrations of liquid-propellant launch vehicles, NASA TN D-5803, 1970.
22. KANA, D.D. and NAGY, A. An experimental study of axisymmetric modes in various propellant tanks containing liquid, DCN 1-9-53-20030, Southwest Research Institute, 1971.
23. GOLDMAN, R.L. and RUDD, T.J. Longitudinal vibration analysis of partially filled ellipsoidal tanks, *J Computers and Structures*, 1973, **3**, pp 205-215.

24. XU, D., HAO, Y. and TANG, G. New pogo analysis method using rational fitting and three-dimensional tank modelling, *AIAA J*, 2015, **53**, (2), pp 405-412.
25. KOHSETSU, Y. Structural system design of liquid rocket, Kyushu University, Japan, Chap. 11, 2013.
26. UJINO, T., SHIMURA, T., KOHSETSU, Y. and NIITSU, M. POGO prevention of H-2 launch vehicle, *AIAA 35th Structural Dynamics and materials Conference*, AIAA-94-1624-CP, 1994, Hilton Head, South Carolina, US.
27. QUINN, S. and SWANSON, L. Overview of the main propulsion system for the NASA Ares I upper stage, *AIAA/ASME/SAE/ASEE Joint Propulsion Conference*, 2009, Denver, Colorado, US.
28. Anonymous. Saturn V flight manual-SA503, MSFC-MAN-503, NASA George C. Marshall Space Flight Centre, 1968.
29. PAN, Z., XING, Y., ZHU, L., DONG, K. and SUN, M. Liquid propellant analogy technique in dynamic modelling of launch vehicle, *Science China*, 2010, **53**, (8), pp 2102-2110.
30. KIM, J., SHIN, S., PARK, J. and KIM, Y. Structural modelling reflected nonlinearity for longitudinal dynamic instability (POGO) analysis of liquid propellant launch vehicles in preliminary design phase, *AIAA SPACE 2015 Conference and Exposition*, 2015, Pasadena, California, US.
31. LARSEN, C.E. NASA experience with pogo in human spaceflight vehicles, *NATO RTO Symposium*, RTO-MP-AVT-152, 2008, Norway.

https://doi.org/10.1017/aer.2017.56 Published online by Cambridge University Press